

RESEARCH ARTICLE

10.1002/2016JD025695

Key Points:

- Decoupled clouds exhibit lower subcloud aerosol and cloud drop concentrations and more impacted by land sources
- Coupled clouds have higher total air-equivalent levels of dissolved nonwater species, with sea salt being dominant
- Nonwater species mass fractions vary significantly between coupled and decoupled clouds in cloud water and droplet residual particles

Correspondence to:

A. Sorooshian,
armin@email.arizona.edu

Citation:

Wang, Z., et al. (2016), Contrasting cloud composition between coupled and decoupled marine boundary layer clouds, *J. Geophys. Res. Atmos.*, 121, 11,679–11,691, doi:10.1002/2016JD025695.

Received 24 JUL 2016

Accepted 13 SEP 2016

Accepted article online 15 SEP 2016

Published online 1 OCT 2016

Contrasting cloud composition between coupled and decoupled marine boundary layer clouds

Zhen Wang¹, Marco Mora Ramirez¹, Hossein Dadashazar¹, Alex B. MacDonald¹, Ewan Crosbie^{2,3}, Kelvin H. Bates⁴, Matthew M. Coggon⁴, Jill S. Craven⁴, Peng Lynch⁵, James R. Campbell⁵, Mojtaba Azadi Aghdam¹, Roy K. Woods⁶, Hafliði Jonsson⁶, Richard C. Flagan⁴, John H. Seinfeld⁴, and Armin Sorooshian^{1,7}

¹Department of Chemical and Environmental Engineering, University of Arizona, Tucson, Arizona, USA, ²NASA Langley Research Center, Hampton, Virginia, USA, ³Universities Space Research Association, Columbia, Maryland, USA, ⁴Division of Chemistry and Chemical Engineering, California Institute of Technology, Pasadena, California, USA, ⁵United States Naval Research Laboratory, Monterey, California, USA, ⁶Naval Postgraduate School, Monterey, California, USA, ⁷Department of Hydrology and Atmospheric Sciences, University of Arizona, Tucson, Arizona, USA

Abstract Marine stratocumulus clouds often become decoupled from the vertical layer immediately above the ocean surface. This study contrasts cloud chemical composition between coupled and decoupled marine stratocumulus clouds for dissolved nonwater substances. Cloud water and droplet residual particle composition were measured in clouds off the California coast during three airborne experiments in July–August of separate years (Eastern Pacific Emitted Aerosol Cloud Experiment 2011, Nucleation in California Experiment 2013, and Biological and Oceanic Atmospheric Study 2015). Decoupled clouds exhibited significantly lower air-equivalent mass concentrations in both cloud water and droplet residual particles, consistent with reduced cloud droplet number concentration and subcloud aerosol ($D_p > 100$ nm) number concentration, owing to detachment from surface sources. Nonrefractory submicrometer aerosol measurements show that coupled clouds exhibit higher sulfate mass fractions in droplet residual particles, owing to more abundant precursor emissions from the ocean and ships. Consequently, decoupled clouds exhibited higher mass fractions of organics, nitrate, and ammonium in droplet residual particles, owing to effects of long-range transport from more distant sources. Sodium and chloride dominated in terms of air-equivalent concentration in cloud water for coupled clouds, and their mass fractions and concentrations exceeded those in decoupled clouds. Conversely, with the exception of sea-salt constituents (e.g., Cl, Na, Mg, and K), cloud water mass fractions of all species examined were higher in decoupled clouds relative to coupled clouds. Satellite and Navy Aerosol Analysis and Prediction System-based reanalysis data are compared with each other, and the airborne data to conclude that limitations in resolving boundary layer processes in a global model prevent it from accurately quantifying observed differences between coupled and decoupled cloud composition.

1. Introduction

The composition of gases, particles, and droplets in and around clouds impacts cloud properties, radiative forcing, the water cycle, and geochemical cycling of nutrients. The degree of coupling between the cloud and the surface layer in a given region is a fundamental property of the cloud system that is expected to impact its composition. Quantifying the effect of coupling on composition is particularly important for marine stratocumulus clouds, which are the dominant cloud type by global area [e.g., Warren *et al.*, 1986], exerting a strong negative net radiative effect [e.g., Stephens and Greenwald, 1991]. Stratocumulus-topped boundary layers are often capped by a strong temperature inversion and are well mixed due to longwave radiative and evaporative cooling at cloud top [e.g., Wood, 2012]. When the negative buoyancy generated at cloud top is not sufficiently strong, the cloud layer can become decoupled from the layer immediately above the ocean [e.g., Nicholls, 1984].

The goal of this study is to determine how the degree of coupling of clouds to the surface layer affects mass concentrations and chemical ratios in cloud water and droplet residual particles for dissolved nonwater substances. While numerous past studies have examined either cloud microphysical properties of stratocumulus clouds in our study region over the eastern Pacific Ocean off the California coast [e.g., Coakley *et al.*, 2000; Durkee *et al.*, 2000; Ferek *et al.*, 2000; Noone *et al.*, 2000; Mechem and Kogan, 2003; Stevens *et al.*, 2003;

Gerber *et al.*, 2005; Sharon *et al.*, 2006; Wang *et al.*, 2008; Lu *et al.*, 2009; Painemal and Minnis, 2012; Modini *et al.*, 2015; Sanchez *et al.*, 2016] or the nature of decoupled marine clouds versus coupled clouds [e.g., Nicholls and Leighton, 1986; Bretherton and Wyant, 1997; Considine, 1997; O'Dowd *et al.*, 2000; Garreaud *et al.*, 2001; Glantz *et al.*, 2003; Bretherton *et al.*, 2010a, 2010b; Berner *et al.*, 2011; Jones *et al.*, 2011; Burleyson *et al.*, 2013; Terai *et al.*, 2014; Dong *et al.*, 2015; Crosbie *et al.*, 2016], none to our knowledge have focused on contrasting composition between coupled and decoupled clouds. It is hypothesized that clouds more strongly coupled to the surface will be more influenced by ocean and ship emissions and less so by continental emissions. Our observations are compared with satellite data and reanalysis data based on the Navy Aerosol Analysis and Prediction System (NAAPS) model to assess the extent to which the model can capture the chemical signature of the two cloud types. The results are intended to motivate more attention to the extent to which clouds are coupled to the surface layer in future studies of cloud composition and aerosol-cloud interactions.

2. Experimental Methods

2.1. Airborne Measurements

Data are analyzed from three flight campaigns using the Center for Interdisciplinary Remotely-Piloted Aircraft Studies Twin Otter based in Marina, CA. The Eastern Pacific Emitted Aerosol Cloud Experiment (E-PEACE) [Russell *et al.*, 2013] included 30 flights between July and August in 2011, the Nucleation in California Experiment (NiCE) [Coggon *et al.*, 2014] included 23 flights between July and August in 2013, and the Biological and Oceanic Atmospheric Study (BOAS) comprised 15 flights in July 2015.

Cloud water was collected with a Mohnen slotted-rod collector [Hegg and Hobbs, 1986]. Details about the collection, storage, and chemical analyses during the three field campaigns are provided elsewhere [Wang *et al.*, 2014]. Briefly, samples were collected over a ~10–30 min duration in high-density polyethylene bottles, with 87, 119, and 29 samples collected in E-PEACE, NiCE, and BOAS, respectively. Samples were tested for pH (Oakton Model 110 pH meter calibrated with pH 4.01 and pH 7.00 buffer solutions), water-soluble composition (Ion Chromatography, IC; Thermo Scientific Dionex ICS—2100 system), and elemental composition (inductively coupled plasma mass spectrometry, ICP-MS; Agilent 7900 Series). The non-sea-salt (NSS) fractions of sulfate and calcium in cloud water were calculated using the relative abundance of sodium to other constituents of sea salt [Seinfeld and Pandis, 2016]. Sodium data presented are from ICP-MS (Na), owing to improved data quality, rather than from IC (Na⁺); it is assumed that most all of Na is in the form of sea salt. Liquid-phase concentrations of dissolved nonwater cloud water species were converted to air-equivalent concentrations based on the average cloud liquid water content (LWC), as measured by a PVM-100 probe [Gerber *et al.*, 1994]. A threshold LWC value of 0.02 g m⁻³ was used to distinguish between cloud and cloud-free air, as has been done in past work in the study region [Prabhakar *et al.*, 2014; Wang *et al.*, 2014].

Droplet residual particle composition data were collected using a compact time-of-flight aerosol mass spectrometer (C-ToF-AMS; Aerodyne) [Drewnick *et al.*, 2005] downstream of a counterflow virtual impactor (CVI; Brechtel Manufacturing Inc.) [Shingler *et al.*, 2012]. The C-ToF-AMS measured nonrefractory aerosol compositions (organics, sulfate, nitrate, and ammonium) for submicrometer aerosol. During the three field experiments, the CVI exhibited a $D_{p,50}$ cutoff size of 11 μm , with a decreasing transmission efficiency as a function of increasing drop size inside the inlet mainly owing to inertial deposition. As already reported by Shingler *et al.* [2012] for the study region, the $D_{p,50}$ of the CVI was sufficiently low to sample the majority of the drop distribution during flights in the study region, with the exception of periods near cloud base, especially when influenced by ship plumes. In cloud-free air, particles were sampled through a subisokinetic aerosol inlet [Hegg *et al.*, 2005].

Size-resolved particle number concentrations were measured with a condensation particle counter (CPC 3010; TSI Inc.; $D_p > 10$ nm) and a passive cavity aerosol spectrometer probe (PCASP; $D_p \sim 0.1$ – 2.6 μm); subcloud sampling data are used in this study as the precloud aerosol. Cloud drop number concentration data were obtained with a cloud aerosol spectrometer (CAS; $D_p \sim 0.6$ – 60 μm) and a forward scattering spectrometer probe (FSSP; $D_p \sim 2$ – 46 μm). CAS data are used for E-PEACE and NiCE, while FSSP data are used for BOAS. Standard meteorological data were also measured, including temperature, winds, and humidity [e.g., Crosbie *et al.*, 2016].

Differentiating between coupled and decoupled clouds requires criteria involving thermodynamic vertical profile data, including quantification of moisture and temperature decoupling metrics and calculating the

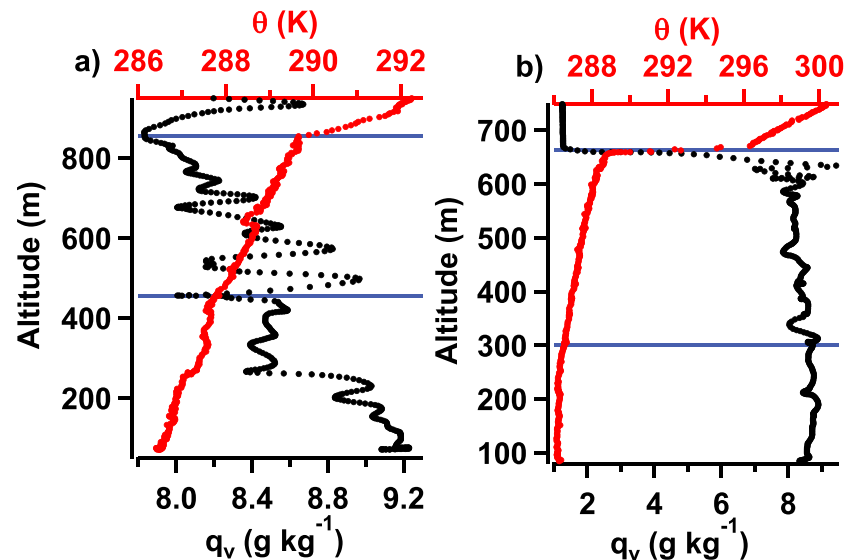


Figure 1. Example of a cloud (a) decoupled from the surface layer and (b) coupled to the surface layer based on vertical profiles of potential temperature and water vapor mixing ratio.

difference between the lifting condensation level and cloud base height [e.g., Jones *et al.*, 2011; Terai *et al.*, 2014; Dong *et al.*, 2015]. Decoupling was initially identified based on observed discontinuities in vertical profiles of thermodynamic properties (potential temperature and water vapor mixing ratio) and aerosol number concentration as measured by the PCASP. When contrasting these clouds to all others, the criteria that emerged for decoupled clouds were that the difference between the bottom and top of the subcloud layer of potential temperature and water vapor mixing ratio had to exceed 1.0 K and 0.6 g kg^{-1} , respectively. All other clouds are considered coupled. In total, we analyzed 13 and 80 decoupled and coupled clouds, respectively. Figure 1 illustrates an example of both a decoupled and coupled cloud based on the aforementioned criteria.

2.2. Vertical Profiles of Particulate Constituents

In order to supplement data from the three aircraft experiments, average vertical profiles of different aerosol constituents were obtained from both the Cloud-Aerosol Lidar with Orthogonal Polarization (CALIOP) and an aerosol reanalysis product, which combines observations with a forecasting model to produce gridded data of atmospheric parameters at a temporal resolution of a few hours. For CALIOP, monthly averaged climatological profile values are used for total and speciated 532 nm aerosol extinction coefficient (km^{-1}) derived at $5^\circ \times 5^\circ$ resolution centered at 37.5°N and -122.5°W ; the methods used to solve these profiles from available quality-assured Version 3 Level 2 Aerosol Profile products are described in Campbell *et al.* [2012]. We specifically report climatological profile data derived between 2006 and 2015 for the months of July and August. Version 3 Level 2 CALIOP aerosol species include “clean marine” (CAL-CM), “dust” (CAL-D), “polluted continental” (CAL-PC), “clean continental” (CAL-CC), “polluted dust” (CAL-PD), and “smoke” (CAL-S) [Omar *et al.*, 2005]. The sum of these species is denoted as “All.”

A decade-long global $1^\circ \times 1^\circ$ and 6-hourly 550 nm aerosol optical thickness (AOT) reanalysis product was recently developed and validated at the Naval Research Laboratory [Lynch *et al.*, 2016]. This reanalysis utilizes a modified version of the Navy Aerosol Analysis and Prediction System (NAAPS) as its core and assimilates quality-controlled retrievals of AOT from Moderate Resolution Imaging Spectroradiometer on Terra and Aqua and the Multiangle Imaging Spectroradiometer on Terra [Zhang and Reid, 2006; Hyer *et al.*, 2011; Shi *et al.*, 2014]. NAAPS characterizes anthropogenic and biogenic fine (ABF, including sulfate and primary and secondary organic aerosols) aerosols, dust, biomass burning smoke, and sea-salt aerosols, the sum of which is denoted as All. The reanalyzed fine (i.e., ABF + smoke) and coarse mode (i.e., sea salt + dust) AOTs at 550 nm are shown to have good agreement with the ground-based global-scale Sun photometer network Aerosol Robotic Network AOTs [Holben *et al.*, 1998]. The three-dimensional NAAPS concentration and extinction data here are extracted from the same NAAPS reanalysis run. Data represent the region encompassed by the following: -125.5° to -122.5°W ; 35.5° to 40.5°N .

Table 1. Summary of Average Environmental Properties Associated With the Decoupled (DC) and Coupled (C) Clouds for Six Different Categories Defined Based on Air Mass Influence and Cloud Base Height^a

Category	Characteristics	Cloud Base Height (m)		Cloud Depth (m)		In-Cloud N _d (cm ⁻³)		Subcloud CPC (cm ⁻³)		Subcloud PCASP (cm ⁻³)	
		DC	C	DC	C	DC	C	DC	C	DC	C
A	Ship-low base	122	136	285	414	42	175	3164	1881	79	304
B	Ship-high base	338	285	320	319	135	240	865	1269	191	360
C	Marine Reference-low base	427	335	400	270	69	149	180	433	98	257
D	Marine Reference-high base	794	766	279	174	82	164	209	343	109	194
E	Land-low base	574	430	343	294	128	163	305	469	91	236
F	Land-high base	808	789	167	244	28	197	369	400	64	224

^aThe number of data points in each category is as follows (coupled/decoupled): A = 12/2; B = 8/1; C = 26/4; D = 14/2; E = 17/3; and F = 3/1.

2.3. Air Back-Trajectory Modeling

Air mass source origins for cloud water samples were identified based on 72 h back trajectories from the NOAA Hybrid Single-Particle Lagrangian Integrated Trajectory (HYSPLIT) model [Stein et al., 2015; Rolph, 2016] ending at the location and altitude of the average point for each sample. HYSPLIT was run using the Global Data Assimilation System data with the “Model vertical velocity” method.

3. Airborne Data Category Definitions

To compare decoupled and coupled clouds, six categories are defined to include cases with similar cloud base heights and air mass influences. Following the criteria previously used by Wang et al. [2014], three air mass categories are as follows: (i) “Ship” = maximum subcloud aerosol concentration as measured by a CPC concentration > 14000 cm⁻³; (ii) “Marine Reference” = maximum subcloud aerosol concentration as measured by a CPC concentration < 1000 cm⁻³; and (iii) “Land” = 72 h back-trajectory contacted land. The first two categories are characterized by an oceanic air source origin, with the primary distinction that the Marine Reference category has an absence of fresh ship emissions. The Land category is associated with continental emissions that impact marine clouds with sources including biogenic emissions, wildfires, and crustal emissions [Coggon et al., 2014; Prabhakar et al., 2014; Maudlin et al., 2015; Sorooshian et al., 2015; Youn et al., 2015]. Each of these three categories is further subdivided into two categories based on cloud base height, resulting in the six categories shown in Table 1. The following cloud base heights were identified as threshold values below and above which cases were categorized as having low base or high base heights, respectively, to maintain a combination of similar numbers of data points and a reasonable separation in height: 250 m (Ship), 600 m (Marine Reference), and 700 m (Land). Cloud base heights for low or high base categories differ between the three air mass categories due to the limited number of decoupled clouds encountered in these campaigns

(Table 1); the comparison between coupled and decoupled clouds at each base height condition within each category is now addressed.

4. Results and Discussion

4.1. Vertical Chemical Profiles From CALIOP

Vertical aerosol extinction profiles from CALIOP are first presented for major aerosol types to provide context for the aircraft data that are for more detailed chemical species (Figure 2). The data begin at a starting altitude of 0.2 km, where the CAL-CM aerosol type dominates the total aerosol extinction coefficient up to between 0.4 and 0.5 km, at which point CAL-PD dominates up to approximately 2.5 km, which surpasses the altitude of the flight data. Most aerosol types decreased in extinction with altitude except for CAL-D (increased up to 0.7 km) and CAL-S

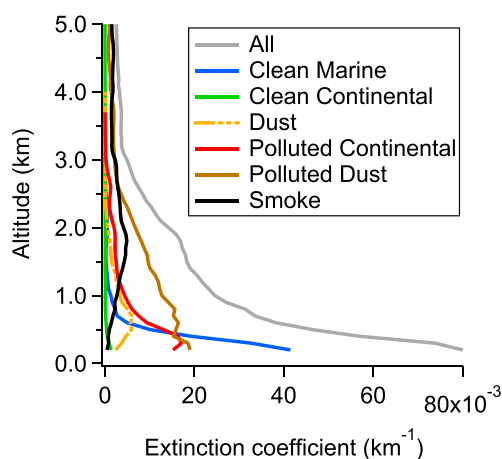


Figure 2. Vertical profiles of aerosol extinction coefficient from CALIOP climatological data for July–August between 2006 and 2015 in the study region.

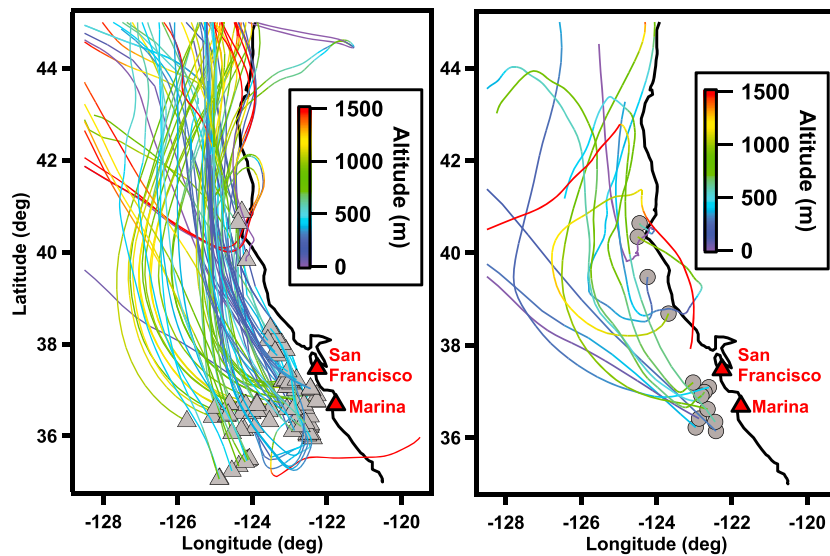


Figure 3. Spatial map of where the cloud water and droplet residual samples were collected in (left) coupled clouds ($n = 80$) (triangles) and (right) decoupled clouds ($n = 13$) (circles) with HYSPLIT 72 h back-trajectories ending at the point of sample collection.

(increased up to 1.8 km), indicative of their presence in the free troposphere from continental sources. CAL-CM decreased at the fastest rate above the surface owing to the surface source of sea salt and effective scavenging at low altitudes. Since the typical boundary layer height in these aircraft campaigns was < 1 km in altitude, it is expected that sea salt is the major component in cloud water; however, a decoupled cloud below 1 km will presumably exhibit a chemical signature impacted more by continental pollution (e.g., dust, smoke, and anthropogenic and biogenic emissions). The CALIOP results are more readily related to cloud water composition (section 4.4) than to droplet residual particle composition data, as the latter data from the C-ToF-AMS represent only nonrefractory species (i.e., excludes sea salt, smoke, and dust).

4.2. Environmental Characteristics

Three-day back-trajectory analysis for the sampled air masses revealed similar pathways generally moving southwards off the western United States coast (Figure 3). Back trajectories for some samples included transsects over land usually to the north of San Francisco. Overall, the HYSPLIT results suggest that the studied clouds were impacted by similar air masses.

Environmental characteristics for decoupled and coupled clouds in each of the six categories are summarized in Table 1. Category averages for cloud base height and cloud depth ranged from 122 to 808 m and 167 to 414 m, respectively. Cloud drop number concentration (N_d) and subcloud number concentration, as measured by the PCASP ($D_p > 100$ nm), were both higher in coupled clouds for all categories owing most likely to influence from ocean and shipping emissions. Another contributing factor to higher N_d in coupled clouds could be higher updraft velocities. One indication that updraft velocity was not the prime driver of the difference in N_d between coupled and decoupled clouds is that the mean vertical wind was lower for coupled clouds in some categories. Coupled stratocumuli over the Azores have also been shown to exhibit higher N_d and surface cloud condensation nucleus concentrations as compared to decoupled stratocumuli [Dong *et al.*, 2015]; that study did not examine updraft velocities though to determine how influential that factor was in governing N_d values. Subcloud number concentrations, as measured by the CPC ($D_p > 10$ nm), were higher for decoupled versus coupled clouds for only one category (Ship-low base) due, most likely, to secondary, organic-rich particles that are formed via gas-to-particle conversion in the free troposphere that tend to have diameters < 100 nm [e.g., Hersey *et al.*, 2009; Coggon *et al.*, 2014]. As larger particles have a greater chance to activate into drops, N_d is better related to subcloud number concentrations measured by the PCASP ($D_p > 100$ nm) as compared to those measured by the CPC ($D_p > 10$ nm).

Table 2. Summary of Constituent Mass Fractions (in Percentage) in Droplet Residual Particles (as Measured by the C-ToF-AMS Downstream of a CVI) and Cloud Water in Decoupled and Coupled Clouds, Based on Cumulative Data for all Six Categories in Table 1^a

		Decoupled	Coupled	Ratio
Droplet residual particles	Organic	54.5%	44.7%	1.22
	SO ₄ ²⁻	23.6%	39.4%	0.60
	NH ₄ ⁺	17.9%	13.0%	1.37
	NO ₃ ⁻	4.0%	2.9%	1.38
Cloud water	Cl ⁻	27.9%	42.6%	0.65
	Na	9.8%	18.6%	0.53
	NO ₃ ⁻	19.8%	12.7%	1.55
	NSS SO ₄ ²⁻	14.5%	12.1%	1.20
	Mg	1.7%	2.7%	0.61
	Glyoxylate	1.5%	0.4%	4.15
	K	0.5%	0.7%	0.71
	MSA	1.7%	1.6%	1.06
	Oxalate	3.4%	1.3%	2.51
	Acetate	3.9%	1.5%	2.69
	Si	7.4%	1.2%	6.32
	Formate	4.1%	1.1%	3.70
	NSS Ca	0.6%	0.3%	2.06
	NO ₂ ⁻	1.4%	0.6%	2.30
Maleate	0.5%	0.4%	1.30	

^aIt is noted that C-ToF-AMS data represent only nonrefractory species and exclude sea salt. "Ratio" = decoupled:coupled mass fraction. Cloud water species in italics were examined using IC, while the rest were examined using ICP-MS.

4.3. Droplet Residual Particle Composition

The focus of the drop residual particle chemical analysis is on chemical ratios (Table 2 and Figure 4) and not absolute mass concentrations owing to uncertainty in their quantification using CVI inlets [Shingler et al., 2012]. CVI data are not available for decoupled clouds in category F.

For decoupled clouds, organics were usually the dominant component, with a cumulative mass fraction average of 0.55 and a category range of 0.32 to 0.88. Aside from having the highest mass fraction in category C (Marine Reference-low base), sulfate was the second most abundant component for category E (mass fraction = 0.06), which consisted of samples obtained farther to the north of the San Francisco area. For categories A/B/D, ammonium was the next most abundant component (mass fraction

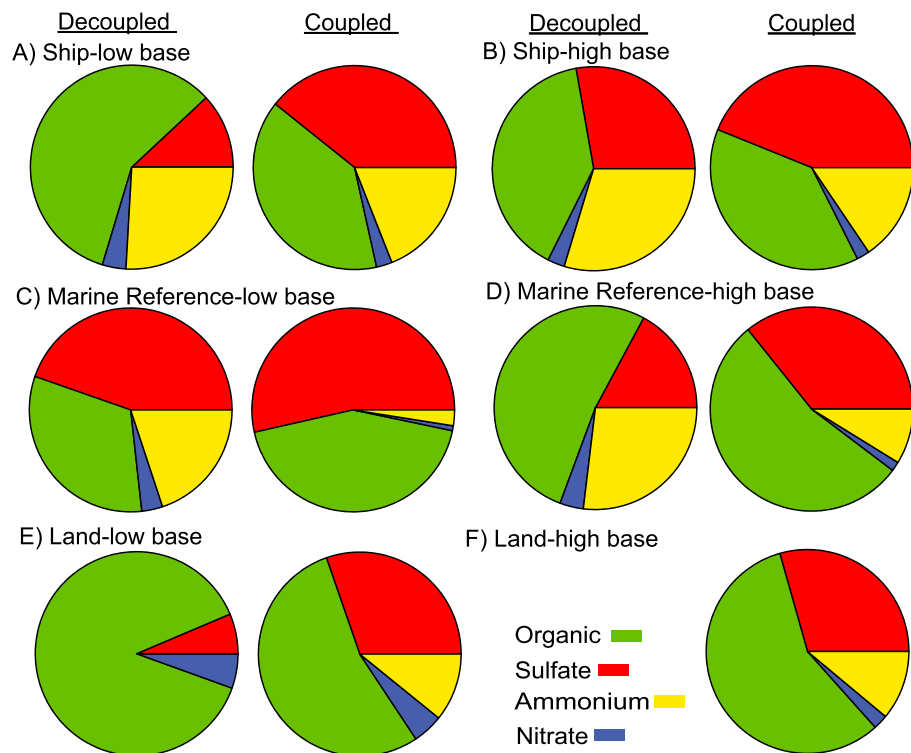


Figure 4. Comparison of droplet residual particle chemical mass fractions, as measured by a C-ToF-AMS downstream of a CVI, for decoupled versus coupled clouds in the six categories (A–F) defined in Table 1. CVI data were not available for decoupled clouds in category F.

Table 3. Cumulative Average Cloud Water Mass Concentration Summary of Species Measured in Decoupled and Coupled Clouds^a

	Units	Decoupled	Coupled	Ratio
<i>Total</i>		2.47	13.38	0.18
<i>Cl⁻</i>		0.76	7.06	0.11
<i>Na</i>		0.36	3.24	0.11
<i>NO₃⁻</i>		0.45	0.87	0.52
<i>NSS SO₄²⁻</i>		0.30	0.85	0.35
<i>Mg</i>		0.06	0.46	0.13
<i>Glyoxylate</i>	μg m ⁻³	0.11	0.27	0.39
<i>K</i>		0.02	0.13	0.17
<i>MSA</i>		0.04	0.12	0.32
<i>Oxalate</i>		0.07	0.11	0.65
<i>Acetate</i>		0.11	0.10	1.10
<i>Si</i>		0.16	0.10	1.66
<i>Formate</i>		0.12	0.08	1.52
<i>NSS Ca</i>		0.02	0.04	0.57
<i>NO₂⁻</i>		0.03	0.03	1.06
<i>Maleate</i>		8.63	30.53	0.28
<i>Fluoride</i>		8.89	23.92	0.37
<i>Pyruvate</i>		7.89	15.09	0.52
<i>Br</i>		2.17	14.36	0.15
<i>I</i>		7.79	9.85	0.79
<i>Fe</i>		5.68	5.70	1.00
<i>Al</i>		5.42	4.97	1.09
<i>Cd</i>		2.80	3.83	0.73
<i>Sr</i>		0.67	3.39	0.20
<i>Cu</i>		1.03	1.61	0.64
<i>Mn</i>	ng m ⁻³	2.25	1.40	1.61
<i>Zn</i>		0.81	1.33	0.61
<i>V</i>		0.25	0.63	0.40
<i>Se</i>		0.17	0.33	0.50
<i>Ni</i>		0.12	0.13	0.93
<i>Ti</i>		0.12	0.12	0.98
<i>Pb</i>		0.03	0.09	0.30
<i>Cr</i>		0.08	0.08	1.01
<i>As</i>		0.02	0.06	0.41
<i>Rb</i>		0.01	0.05	0.29
<i>Co</i>		0.02	0.02	1.55

^aRatio = decoupled:coupled concentration. Species in italics were examined using IC, while the rest were examined using ICP-MS. Species are listed in decreasing order of value for the coupled category.

organic:sulfate ratio versus that below and in clouds [e.g., Sorooshian *et al.*, 2007; Coggon *et al.*, 2012]. The source of organics aloft includes biogenic and wildfire emissions from the northwestern United States [Coggon *et al.*, 2012, 2014]. The average organic:sulfate mass concentration ratio for decoupled clouds (116.1) was approximately 10 times larger than that in coupled clouds (11.7). The high value for decoupled clouds was driven by two individual samples with values of 422.5 and 547.4; when omitting those two samples, the decoupled ratio becomes 23.8, which still is more than twice that of coupled clouds. Particles in the study region with higher organic:sulfate ratios are less hygroscopic, as has previously been shown by comparisons of aerosol particles above coupled cloud tops versus below bases both in the subsaturated [Hersey *et al.*, 2009] and supersaturated regime [Crosbie *et al.*, 2016]. Thus, the extent to which clouds are decoupled from the surface layer has implications for hygroscopic, and thus radiative, properties of particles in and around clouds.

4.4. Cloud Water Composition

4.4.1. Cumulative Concentration Data

Tables 2 and 3 summarize mass fractions and air-equivalent mass concentrations, respectively, of cloud water constituents for decoupled and coupled clouds. Total cloud water mass concentration is calculated as the sum of the following species: (from IC) NSS SO₄²⁻, NO₃⁻, Cl⁻, NO₂⁻, glyoxylate, acetate, formate,

range: 0.26–0.30). Nitrate was the least abundant component, with a mass fraction maximum of only 0.05 in category E. Nitrate is prone to volatilization in the CVI inlet, and it is present in coarse and/or refractory particles that are undetectable by the C-ToF-AMS [e.g., Prabhakar *et al.*, 2014], and thus, its reported values most likely represent a lower bound.

For coupled clouds, organics are the dominant contributor to droplet residual particle mass for three of six categories (D–F), with a cumulative mass fraction average of 0.45 and category range of 0.38 to 0.57. The main difference between coupled and decoupled clouds can be distinguished by the sulfate mass fraction, which is generally higher for coupled clouds (0.39 versus 0.24) with lower relative amounts of the other constituents. Sulfate stems from precursor emissions emitted at the ocean surface, including dimethylsulfide (DMS) and SO₂ from shipping. Consequently, sulfate exhibited a higher mass fraction than organics for the two ship categories (A and B). As in decoupled clouds, nitrate was the least abundant constituent of droplet residual particles (mass fraction average = 0.03) based on C-ToF-AMS data.

Previous work in the study region has shown that aerosol particles above cloud top generally have a higher

methanesulfonate (MSA), pyruvate, maleate, oxalate, fluoride, and lactate and (from ICP-MS) Na, Mg, Al, Si, K, NSS Ca, Ti, V, Cr, Mn, Fe, Co, Ni, Cu, Zn, As, Se, Br, Rb, Sr, Cd, I, and Pb. Total cloud water air-equivalent mass concentration was significantly higher for coupled versus decoupled clouds, exceeding a factor of 5 based on cumulative data (13.38 versus $2.47 \mu\text{g m}^{-3}$, respectively).

Due to sea-salt emissions, chloride, followed by sodium, contributed the most to cloud water mass for coupled clouds, each being nearly an order of magnitude higher in concentration than in decoupled clouds. This result is consistent with the vertical profiles of aerosol extinction from CALIOP (Figure 2), which show the dominance of the CAL-CM aerosol type in the first few hundred meters above the surface in the region where the coupled cloud measurements were conducted. The combined mass fraction of chloride and sodium relative to total mass is 0.61 and 0.38 for coupled and decoupled clouds, respectively. There is no significant difference in the Cl:Na molar ratio, with values of 1.15 and 1.13 for the coupled and decoupled clouds, respectively. These values are close to those characteristic of natural sea salt, 1.17, and thus, there is no obvious evidence of significant chloride depletion owing to acidic constituents, even though cloud water pH was 4.26 and 4.48 for coupled and decoupled cloud samples, respectively. Furthermore, the similarity in the ratios is suggestive of sea salt having been lofted above the surface layer [e.g., Lewis and Schwartz, 2004; Hara *et al.*, 2014] in decoupled clouds at some earlier point.

Nitrate and NSS sulfate are the third and fourth most abundant components in coupled clouds, respectively. Regional sources of nitrate include ship exhaust, ocean sea spray and biogenic emissions, and wildfires [Prabhakar *et al.*, 2014]. Nitrate is more abundant than NSS sulfate in cloud water, in contrast to droplet residual particle measurements, likely as a result of a combination of dissolution of HNO_3 , activation of coarse and/or refractory particles undetectable by the C-ToF-AMS, and the absence of volatilization effects that are associated with heating in the CVI inlet [Prabhakar *et al.*, 2014].

A few of the less abundant species in Table 3 are more than 5 times enhanced in coupled clouds relative to decoupled clouds, including K, Sr, Br, and Mg. These species have a mix of natural and anthropogenic sources in the study region [Wang *et al.*, 2014]. MSA was more than 3 times higher in concentration in coupled clouds presumably due to DMS emissions from the ocean surface. With the exception of acetate and formate, organic acids in Table 3 (glyoxylate, oxalate, maleate, and pyruvate) were higher in concentration in coupled clouds, particularly maleate (by over a factor of 3.5) that forms from aromatic hydrocarbon oxidation [Rogge *et al.*, 1993], sources of which in the study region include diesel and gasoline engines. Maleate is a precursor to glyoxylate, the chief aqueous precursor to oxalate [e.g., Sorooshian *et al.*, 2013], the latter two of which are ~ 2.6 and ~ 1.5 times higher in concentration, respectively, in coupled clouds than in decoupled ones.

In decoupled clouds, species enhanced in concentration relative to coupled clouds include formate, Si, Co, Mn, nitrite, Al, Cr, and acetate by factors reaching as high as 1.66, with the difference in mean concentration being statistically significant (t test with a two-tailed p value threshold of 0.05) for the first four species. These species are influenced from continental sources near the study region such as crustal matter, which is the likely source of Si [Coggon *et al.*, 2014; Wang *et al.*, 2014]. Continental air masses almost certainly influence the composition of decoupled clouds owing to their general presence in the free troposphere of the region [e.g., Coggon *et al.*, 2014]. As air masses impacting the study region were transported southward along the coast (Figure 3), forest emissions likely influenced their compositions, especially north of central CA [Coggon *et al.*, 2014]. Formate is one of the most enhanced species in decoupled clouds versus coupled ones (factor of 1.52). Formate originates from formic acid, 90% of which is biogenic in origin, especially from boreal forests [Stavrakou *et al.*, 2012]. CALIOP data also show that above approximately 0.4–0.5 km, CAL-D, CAL-PD, and CAL-PC aerosol types exceed CAL-CM aerosol in terms of extinction coefficient, confirming that clouds impacted by free tropospheric air in the region exhibit greater influence from continental air than by sea salt. In summary, the results in Table 3 indicate that the decoupled clouds have much smaller air-equivalent mass concentrations of the species studied, except for a few species with likely continental sources, owing to the large size of sea-salt particles driving mass concentrations much higher in coupled clouds.

4.4.2. Cumulative Mass Fraction Data

Because microphysical properties, such as aerosol hygroscopicity, depend on relative concentrations of chemical constituents, differences in mass fractions in cloud water are discussed here (Table 2) with a focus on those species accounting for most of the total mass. In decoupled clouds, mass fractions of sodium and chloride are reduced relative to coupled clouds by factors of ~ 1.9 and ~ 1.5 , respectively. As these two species

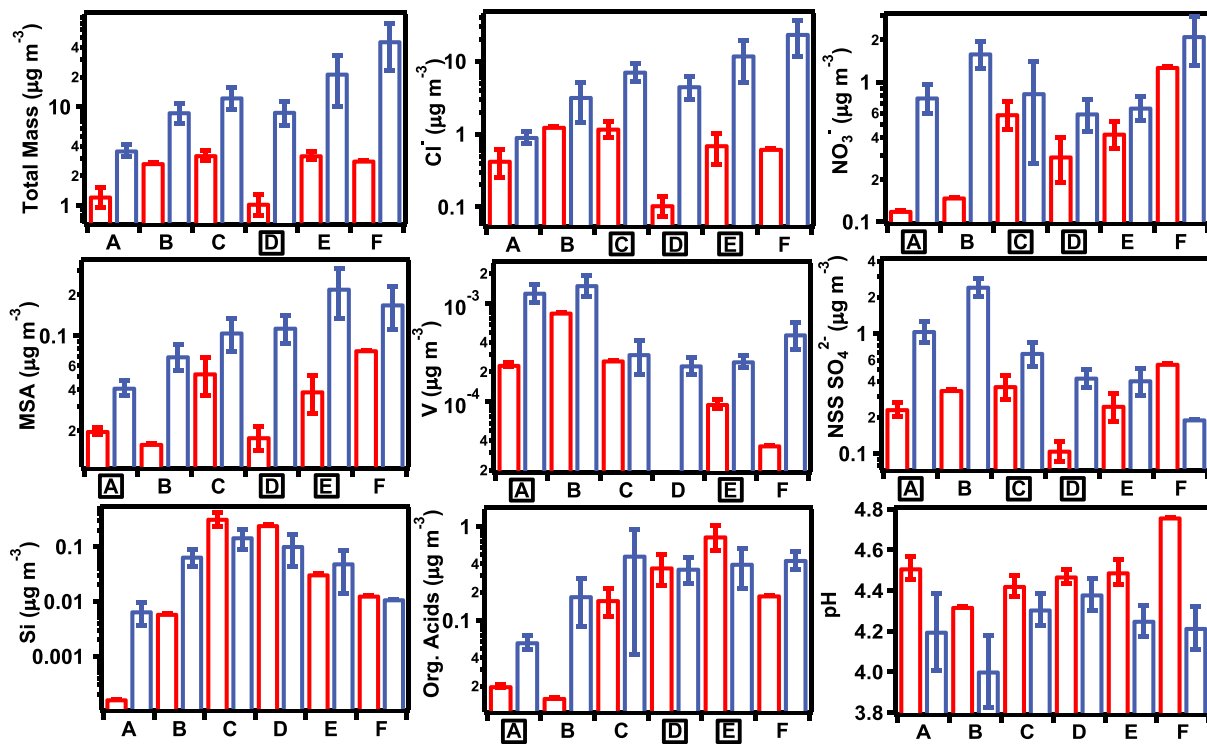


Figure 5. Comparison of cloud water parameters between coupled (blue) and decoupled (red) clouds for the six categories (A–F) defined in Table 1. Category labels with a box around them indicate that the difference between the two means of that category is statistically significant (two-sample *t* test with a two-tailed *p* value threshold of 0.05).

dominate the mass concentration in coupled clouds, the mass fractions of all species except for Mg and K in Table 2 are higher for decoupled clouds. Mg and K are the fourth and sixth most abundant components of natural sea salt by mass after chloride, sodium, and sulfate [e.g., Seinfeld and Pandis, 2016]. Thus, they are expected to preferentially impact coupled clouds. The greatest enhancements in the mass fraction in decoupled versus coupled clouds are for carboxylic acids (glyoxylate, formate, oxalate, and acetate), nitrite, Si, and NSS Ca with enhancement factors ranging from 2.06 to 6.32.

4.4.3. Categorical Chemical Differences

Figure 5 contrasts cloud water chemical data for coupled and decoupled clouds for each of the six categories of Table 1, with statistically significant (*t* test with a two-tailed *p* value threshold of 0.05) differences in mean values highlighted on each x axis. Although many differences are not statistically significant owing largely to limited data points in the decoupled categories, relative differences are still of importance to discuss. Total mass concentrations are highest in coupled clouds in categories E to F (Land-low base and Land-high base), and highest in categories C/E (Marine Reference-low base; Land-low base) for decoupled clouds. Analysis of the various constituents in Figure 5 explains this result. For coupled clouds, chloride is highest in concentration for categories E and F, thus driving the total mass concentration to maximum levels. Nitrate is also highest in category F owing to its association with sea salt in the study region [Prabhakar et al., 2014]. MSA levels are also highest in categories E and F, suggesting that biogenic emissions contribute in addition to direct emission of sea spray. While ship emissions are shown to be less influential to cloud water mass concentrations relative to ocean emissions (e.g., sea salt), it is worth noting that the ship exhaust tracer, V, was most enhanced in categories A and B (Ship-low base and Ship-high base) as expected for coupled clouds. NSS sulfate is highest in category B due to the contribution from ship-derived SO₂.

For decoupled clouds, the largest contributors to the peak total mass in category C are chloride, followed by nitrate, while the order of these two species is reversed for category E. Representative tracer species for continental crustal matter, namely, Si and NSS Ca (not shown in Figure 5) [Wang et al., 2014], clearly exhibit a peak concentration in category C. Interestingly, the coupled clouds also show the highest Si concentration in the same categories as the decoupled clouds, albeit at lower concentrations, indicative of the influence of

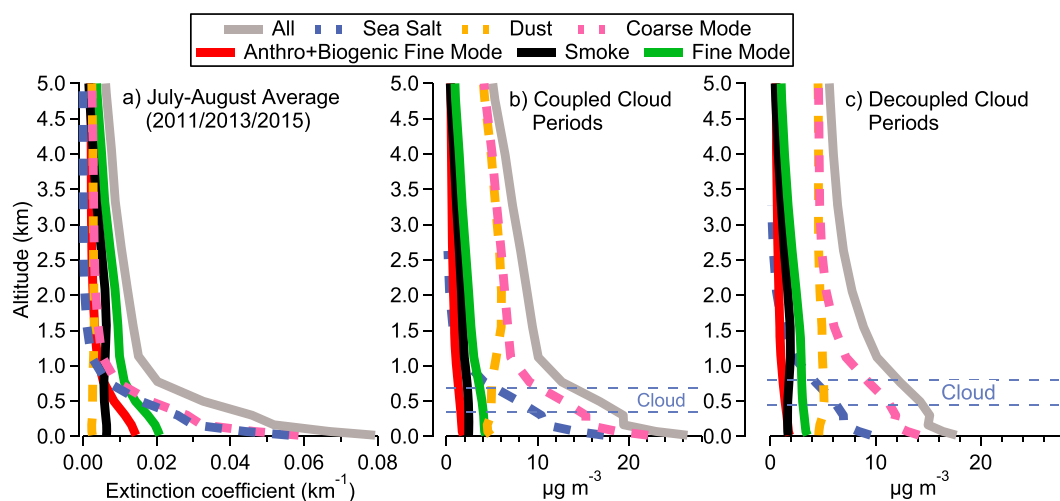


Figure 6. Vertical profile of aerosol constituents from the NAAPS-based reanalysis product. (a) Profiles of aerosol extinction coefficient for July and August for the three summers that field campaign data were analyzed. (b) Profile of aerosol mass concentrations for the times coinciding with the coupled clouds examined. (c) Profile of aerosol mass concentrations for the times coinciding with the decoupled clouds examined. The horizontal bars in Figures 6b and 6c correspond to the average cloud base and top heights for coupled and decoupled clouds.

continental air for coupled clouds near the coast; CALIOP profiles showing enhanced levels of CAL-PD and CAL-PC aerosol types in the first few hundred meters above the surface support this inference. The total concentration peak in category E for decoupled clouds appears to be influenced by different sources when compared to category C. More specifically, while crustal matter tracer species are much lower in category E, concentrations of organic acids are much higher. The cumulative concentration of acetate, formate, pyruvate, glyoxylate, oxalate, and maleate was $0.79 \mu\text{g m}^{-3}$, exceeding by more than a factor of 2 the concentration of any other category for decoupled clouds. Formate and acetate were the two most abundant organic acids in category E, with their source likely being biogenic emissions from upwind continental areas as noted in previous work [Coggon *et al.*, 2014].

Cloud water pH is higher in decoupled clouds than coupled ones for all six categories, owing presumably to a lower impact of acidic compounds from shipping combined with increased contributions of basic compounds coming upwind from the continent. The lowest pH (4.0) occurred for coupled clouds in category B (Ship-high base), which exhibits the highest V concentration and thus shipping influence. The highest pH (4.76) occurred for decoupled clouds in category F (Land-high base), consistent with past work showing that cloud water pH is higher when influenced by continental air masses enriched with crustal species, especially Si, in the study region [Wang *et al.*, 2014].

4.5. Reanalysis Data

It is of interest to contrast vertically resolved chemical profiles from the NAAPS-based reanalysis product for the same time periods of the decoupled and coupled clouds. NAAPS can resolve aerosol vertical profiles on a temporal/spatial scales consistent with the flights described. CALIOP observations cannot be used in this capacity as they are dependent on orbital configurations and cannot provide measurements near the flights. The NAAPS reanalysis was specifically designed as an aerosol optical depth product, with little tuning done vertically to ensure vertical profiling skill explicitly [Lynch *et al.*, 2016]. Fortunately, Figure 6a demonstrates that the reanalysis data, when averaged for July–August for the three experiment years (2011, 2013, and 2015), generally agree with the climatological CALIOP profiles. Similar to CALIOP observations, the reanalysis data show that the maximum total extinction coefficient (denoted as All) is $\sim 0.08 \text{ km}^{-1}$ near the surface. Sea salt accounts for most extinction below about 0.5 km, above which other constituents dominate, mainly fine mode components (smoke, ABF).

Figures 6b and 6c show mass concentration vertical profiles for the same time as when coupled and decoupled cloud measurements, respectively, were conducted. Rather than extinction coefficients, mass concentrations are shown for a direct comparison with the cloud water measurements. The relative concentration variations

with altitude are nearly identical between the composite profiles for coupled and decoupled clouds. Perhaps, the most significant difference is the much higher sea-salt concentrations (by up to a factor of 1.8) in the lowest few hundred meters for the coupled composite profile owing to stronger surface winds (at 10 m) as predicted by the model. The average near-surface (<100 m) wind speeds coinciding with measurements of the coupled and decoupled clouds were 4.8 and 4.6 m s⁻¹, respectively, indicating that at least in the spatial range of where the aircraft flew, there was no significant difference in wind speed unlike in the model.

To compare the composite profiles to the cloud composition data, the mass fractions of the four main components (ABF, sea salt, dust, and smoke) are compared between coupled and decoupled composite profiles at cloud-relevant altitudes for each category. In contrast to the measurements (Table 2), the reanalysis mass fractions are nearly identical for the two cloud types (coupled/decoupled): ABF = 0.10/0.10, sea salt = 0.40/0.41, dust = 0.34/0.37, and smoke = 0.16/0.12. As sea salt is the most abundant cloud water constituent, its modeled and observed mass concentrations at cloud-relevant altitudes for coupled and decoupled clouds are as follows (modeled/observed): 6.1/10.3 μg m⁻³ for coupled and 5.8/1.1 μg m⁻³ for decoupled clouds, where the observed value is calculated as the sum of Na and Cl⁻. While the modeled and measured concentrations are within an order of magnitude, the remaining discrepancy is indicative of the current limitations of the resolution of a global model for boundary layer processes, leading to the observed difference in coupled and decoupled composition.

5. Conclusions

Aircraft measurements of cloud water and droplet residual particle composition over the eastern Pacific Ocean off the California coast between July and August of 3 years (2011, 2013, and 2015) are examined in this work for clouds decoupled from and coupled to the surface layer. While differences are expected between these two cloud conditions, this work provides quantitative data. The main findings of this work are as follows:

1. Total mass concentration of measured constituents in droplet residual particles and cloud water was significantly enhanced in coupled clouds, coincident with higher N_d and subcloud number concentrations as measured by the PCASP ($D_p > 100$ nm). This can be explained by the stronger influence on coupled clouds by ocean and shipping emissions.
2. Organics and sulfate were the most abundant components in droplet residual particles, with sulfate mass fraction generally being higher in coupled versus decoupled clouds (0.39 versus 0.24), unlike organics, ammonium, and nitrate. Consequently, organic:sulfate ratios are much larger in decoupled clouds, resulting in less hygroscopic aerosol particles.
3. Of the 35 cloud water constituents analyzed, 27 were higher in concentration in coupled clouds, with chloride, followed by sodium, being the most abundant owing to sea-salt emissions. The remaining eight constituents (acetate, formate, Si, nitrite, Al, Mn, Cr, and Co) that were more enhanced in decoupled clouds are consistent with the influence of continental air masses in the free troposphere of the region.
4. With exception of components associated with sea salt (e.g., Cl, Na, Mg, and K), cloud water mass fractions of all species examined were higher in decoupled clouds relative to coupled clouds. Species with the largest enhancement in mass fraction in decoupled clouds included numerous carboxylic acids (glyoxylate, formate, oxalate, and acetate), nitrite, Si, and NSS Ca. Cloud water pH was also higher in decoupled clouds, which has implications for heterogeneous chemistry such as affecting sulfur oxidation rates [e.g., Collett *et al.*, 1994].
5. Limitations in resolving boundary layer processes in a global model, based on NAAPS-based reanalysis data, prevent it from accurately quantifying observed differences between coupled and decoupled cloud composition.

Clouds detached from the surface layer are shown here to have significantly different cloud composition, which, in turn, impacts the nature of the chemical processing that takes place in those clouds, microphysical cloud properties, and the physicochemical properties of aerosol particles after cloud drop evaporation.

References

- Berner, A. H., C. S. Bretherton, and R. Wood (2011), Large-eddy simulation of mesoscale dynamics and entrainment around a pocket of open cells observed in VOCALS-REx RF06, *Atmos. Chem. Phys.*, 11(20), 10,525–10,540.
- Bretherton, C. S., and M. C. Wyant (1997), Moisture transport, lower-tropospheric stability, and decoupling of cloud-topped boundary layers, *J. Atmos. Sci.*, 54(1), 148–167.

Acknowledgments

This work was funded by ONR grants N00014-11-1-0783, N00014-10-1-0200, N00014-04-1-0118, N00014-10-1-0811, and N00014-16-1-2567 and NSF grant AGS-1008848. Field campaign data used for this study can be obtained at u.arizona.edu/~armin, and questions about those data should be directed to the corresponding author (armin@email.arizona.edu). The NAAPS reanalysis data are available at http://usgodae.org/cgi-bin/datalist.pl?dset=nrl_naaps_reanalysis&summary=Go; the data on that server are updated as model improvements are made and reruns are completed. CALIOP data are available at the following website: <https://eosweb.larc.nasa.gov/>.

- Bretherton, C. S., R. Wood, R. C. George, D. Leon, G. Allen, and X. Zheng (2010a), Southeast Pacific stratocumulus clouds, precipitation and boundary layer structure sampled along 20 degrees S during VOCALS-REx, *Atmos. Chem. Phys.*, *10*(21), 10,639–10,654.
- Bretherton, C. S., J. Uchida, and P. N. Blossey (2010b), Slow manifolds and multiple equilibria in stratocumulus-capped boundary layers, *J. Adv. Model Earth Syst.*, *2*, doi:10.3894/JAMES.2010.2.14.
- Burleyson, C. D., S. P. de Szoeko, S. E. Yuter, M. Wilbanks, and W. A. Brewer (2013), Ship-based observations of the diurnal cycle of Southeast Pacific marine stratocumulus clouds and precipitation, *J. Atmos. Sci.*, *70*(12), 3876–3894.
- Campbell, J. R., et al. (2012), Evaluating nighttime CALIOP 0.532 μm aerosol optical depth and extinction coefficient retrievals, *Atmos. Meas. Tech.*, *5*(9), 2143–2160.
- Coakley, J. A., et al. (2000), The appearance and disappearance of ship tracks on large spatial scales, *J. Atmos. Sci.*, *57*(16), 2765–2778.
- Coggon, M. M., et al. (2012), Ship impacts on the marine atmosphere: Insights into the contribution of shipping emissions to the properties of marine aerosol and clouds, *Atmos. Chem. Phys.*, *12*(18), 8439–8458, doi:10.5194/acp-12-8439-2012.
- Coggon, M. M., A. Sorooshian, Z. Wang, J. S. Craven, A. R. Metcalf, J. J. Lin, A. Nenes, H. H. Jonsson, R. C. Flagan, and J. H. Seinfeld (2014), Observations of continental biogenic impacts on marine aerosol and clouds off the coast of California, *J. Geophys. Res. Atmos.*, *119*, 6724–6748, doi:10.1002/2013JD021228.
- Collett, J. L., A. Bator, X. Rao, and B. B. Demoz (1994), Acidity variations across the cloud drop size spectrum and their influence on rates of atmospheric sulfate production, *Geophys. Res. Lett.*, *21*, 2393–2396, doi:10.1029/94GL02480.
- Considine, G. D. (1997), Modeling the diurnal variability in cloud microphysics in boundary layer clouds, *J. Geophys. Res.*, *102*, 1717–1726, doi:10.1029/96JD02997.
- Crosbie, E., et al. (2016), Stratocumulus cloud clearings and notable thermodynamic and aerosol contrasts across the clear-cloudy interface, *J. Atmos. Sci.*, *73*(3), 1083–1099.
- Dong, X. Q., A. C. Schwantes, B. K. Xi, and P. Wu (2015), Investigation of the marine boundary layer cloud and CCN properties under coupled and decoupled conditions over the Azores, *J. Geophys. Res. Atmos.*, *120*, 6179–6191, doi:10.1002/2014JD022939.
- Drewnick, F., et al. (2005), A new time-of-flight aerosol mass spectrometer (TOF-AMS)—Instrument description and first field deployment, *Aerosol Sci. Technol.*, *39*(7), 637–658, doi:10.1080/02786820500182040.
- Durkee, P. A., et al. (2000), The impact of ship-produced aerosols on the microstructure and albedo of warm marine stratocumulus clouds: A test of MAST hypotheses 1i and 1ii, *J. Atmos. Sci.*, *57*(16), 2554–2569.
- Ferek, R. J., et al. (2000), Drizzle suppression in ship tracks, *J. Atmos. Sci.*, *57*(16), 2707–2728.
- Garreaud, R. D., J. Rutllant, J. Quintana, J. Carrasco, and P. Minnis (2001), CIMAR-5: A snapshot of the lower troposphere over the subtropical southeast Pacific, *Bull. Am. Meteorol. Soc.*, *82*(10), 2193–2207.
- Gerber, H., B. G. Arends, and A. S. Ackerman (1994), New microphysics sensor for aircraft use, *Atmos. Res.*, *31*(4), 235–252.
- Gerber, H., G. Frick, S. P. Malinowski, J. L. Brenguier, and F. Burnet (2005), Holes and entrainment in stratocumulus, *J. Atmos. Sci.*, *62*(2), 443–459.
- Glantz, P., K. J. Noone, and S. R. Osborne (2003), Scavenging efficiencies of aerosol particles in marine stratocumulus and cumulus clouds, *Q. J. Roy. Meteor. Soc.*, *129*(590), 1329–1350.
- Hara, K., M. Hayashi, M. Yabuki, M. Shiobara, and C. Nishita-Hara (2014), Simultaneous aerosol measurements of unusual aerosol enhancement in the troposphere over Syowa Station, Antarctica, *Atmos. Chem. Phys.*, *14*(8), 4169–4183.
- Hegg, D. A., and P. V. Hobbs (1986), Studies of the mechanisms and rate with which nitrogen species are incorporated into cloud water and precipitation, Second Annual Report on Project CAPA-21-80 to the Coordinating Research Council.
- Hegg, D., D. Covert, H. Jonsson, and P. Covert (2005), Determination of the transmission efficiency of an aircraft aerosol inlet, *Aerosol Sci. Technol.*, *39*(10), 966–971, doi:10.1080/02786820500377814.
- Hersey, S. P., A. Sorooshian, S. M. Murphy, R. C. Flagan, and J. H. Seinfeld (2009), Aerosol hygroscopicity in the marine atmosphere: A closure study using high-time-resolution, multiple-RH DASH-SP and size-resolved C-ToF-AMS data, *Atmos. Chem. Phys.*, *9*(7), 2543–2554.
- Holben, B. N., et al. (1998), AERONET—A federated instrument network and data archive for aerosol characterization, *Remote Sens. Environ.*, *66*(1), 1–16.
- Hyer, E. J., J. S. Reid, and J. Zhang (2011), An over-land aerosol optical depth data set for data assimilation by filtering, correction, and aggregation of MODIS Collection 5 optical depth retrievals, *Atmos. Meas. Tech.*, *4*(3), 379–408.
- Jones, C. R., C. S. Bretherton, and D. Leon (2011), Coupled vs. decoupled boundary layers in VOCALS-REx, *Atmos. Chem. Phys.*, *11*(14), 7143–7153.
- Lewis, E. R., and S. E. Schwartz (2004), *Sea Salt Aerosol Production: Mechanisms, Methods, Measurements and Models—A Critical Review*, *Geophys. Monograph*, vol. 152, pp. 413, AGU, Washington, D. C.
- Lu, M. L., A. Sorooshian, H. H. Jonsson, G. Feingold, R. C. Flagan, and J. H. Seinfeld (2009), Marine stratocumulus aerosol-cloud relationships in the MASE-II experiment: Precipitation susceptibility in eastern Pacific marine stratocumulus, *J. Geophys. Res.*, *114*, D24203, doi:10.1029/2009JD012774.
- Lynch, P., et al. (2016), An 11-year global gridded aerosol optical thickness reanalysis (v1.0) for atmospheric and climate sciences, *Geosci. Model Dev.*, *9*(4), 1489–1522.
- Maudlin, L. C., Z. Wang, H. H. Jonsson, and A. Sorooshian (2015), Impact of wildfires on size-resolved aerosol composition at a coastal California site, *Atmos. Environ.*, *119*, 59–68.
- Mechem, D. B., and Y. L. Kogan (2003), Simulating the transition from drizzling marine stratocumulus to boundary layer cumulus with a mesoscale model, *Mon. Weather Rev.*, *131*(10), 2342–2360.
- Modini, R. L., et al. (2015), Primary marine aerosol-cloud interactions off the coast of California, *J. Geophys. Res. Atmos.*, *120*, 4282–4303, doi:10.1002/2014JD022963.
- Nicholls, S. (1984), The dynamics of stratocumulus—Aircraft observations and comparisons with a mixed layer model, *Q. J. Roy. Meteor. Soc.*, *110*(466), 783–820.
- Nicholls, S., and J. Leighton (1986), An observational study of the structure of stratiform cloud sheets .1. Structure, *Q. J. Roy. Meteor. Soc.*, *112*(472), 431–460.
- Noone, K. J., et al. (2000), A case study of ship track formation in a polluted marine boundary layer, *J. Atmos. Sci.*, *57*(16), 2748–2764.
- O'Dowd, C. D., J. A. Lowe, and M. H. Smith (2000), The effect of clouds on aerosol growth in the rural atmosphere, *Atmos. Res.*, *54*(4), 201–221.
- Omar, A. H., J.-G. Won, D. M. Winker, S.-C. Yoon, O. Dubovik, and M. P. McCormick (2005), Development of global aerosol models using cluster analysis of Aerosol Robotic Network (AERONET) measurements, *J. Geophys. Res.*, *110*, D10S14, doi:10.1029/2004JD004874.
- Painemal, D., and P. Minnis (2012), On the dependence of albedo on cloud microphysics over marine stratocumulus clouds regimes determined from Clouds and the Earth's Radiant Energy System (CERES) data, *J. Geophys. Res.*, *117*, D06203, doi:10.1029/2011JD017120.
- Prabhakar, G., B. Ervens, Z. Wang, L. C. Maudlin, M. M. Coggon, H. H. Jonsson, J. H. Seinfeld, and A. Sorooshian (2014), Sources of nitrate in stratocumulus cloud water: Airborne measurements during the 2011 E-PEACE and 2013 NICE studies, *Atmos. Environ.*, *97*, 166–173.

- Rogge, W. F., M. A. Mazurek, L. M. Hildemann, G. R. Cass, and B. R. T. Simoneit (1993), Quantification of urban organic aerosols at a molecular-level—Identification, abundance and seasonal-variation, *Atmos. Environ.*, *27*(8), 1309–1330.
- Rolph, G. D. (2016), Real-time Environmental Applications and Display sYstem (READY) Website (<http://ready.arl.noaa.gov>). NOAA Air Resources Laboratory, Silver Spring, Md.
- Russell, L. M., et al. (2013), Eastern Pacific emitted aerosol cloud experiment, *Bull. Am. Meteorol. Soc.*, *94*(5), 709–729.
- Sanchez, K. J., et al. (2016), Meteorological and aerosol effects on marine cloud microphysical properties, *J. Geophys. Res. Atmos.*, *121*, 4142–4161, doi:10.1002/2015JD024595.
- Seinfeld, J. H., and S. N. Pandis (2016), *Atmospheric Chemistry and Physics*, 3rd ed., Wiley-Interscience, New York.
- Sharon, T. M., B. A. Albrecht, H. H. Jonsson, P. Minnis, M. M. Khaiyer, T. M. van Reken, J. Seinfeld, and R. Flagan (2006), Aerosol and cloud microphysical characteristics of rifts and gradients in maritime stratocumulus clouds, *J. Atmos. Sci.*, *63*(3), 983–997.
- Shi, Y., J. Zhang, J. S. Reid, B. Liu, and E. J. Hyer (2014), Critical evaluation of cloud contamination in the MISR aerosol products using MODIS cloud mask products, *Atmos. Meas. Tech.*, *7*(6), 1791–1801.
- Shingler, T., et al. (2012), Characterization and airborne deployment of a new counterflow virtual impactor, *Atmos. Meas. Tech.*, *5*, 1515–1541, doi:10.5194/amtd-5-1515-2012.
- Sorooshian, A., M. L. Lu, F. J. Brechtel, H. Jonsson, G. Feingold, R. C. Flagan, and J. H. Seinfeld (2007), On the source of organic acid aerosol layers above clouds, *Environ. Sci. Technol.*, *41*(13), 4647–4654.
- Sorooshian, A., Z. Wang, M. M. Coggon, H. H. Jonsson, and B. Ervens (2013), Observations of sharp oxalate reductions in stratocumulus clouds at variable altitudes: Organic acid and metal measurements during the 2011 E-PEACE campaign, *Environ. Sci. Technol.*, *47*(14), 7747–7756.
- Sorooshian, A., E. Crosbie, L. C. Maudlin, J. S. Youn, Z. Wang, T. Shingler, A. M. Ortega, S. Hersey, and R. K. Woods (2015), Surface and airborne measurements of organosulfur and methanesulfonate over the western United States and coastal areas, *J. Geophys. Res. Atmos.*, *120*, 8535–8548, doi:10.1002/2015JD023822.
- Stavrakou, T., et al. (2012), Satellite evidence for a large source of formic acid from boreal and tropical forests, *Nat. Geosci.*, *5*(1), 26–30.
- Stein, A. F., R. R. Draxler, G. D. Rolph, B. J. B. Stunder, M. D. Cohen, and F. Ngan (2015), NOAA's HYSPLIT atmospheric transport and dispersion modeling system, *Bull. Am. Meteorol. Soc.*, *96*(12), 2059–2077.
- Stephens, G. L., and T. J. Greenwald (1991), Observations of the Earth's radiation budget in relation to atmospheric hydrology. Part II: Cloud effects and cloud feedback, *J. Geophys. Res.*, *96*, 15,325–15,340, doi:10.1029/91JD00972.
- Stevens, B., et al. (2003), Dynamics and chemistry of marine stratocumulus—DYCOMS-II, *Bull. Am. Meteorol. Soc.*, *84*(5), 579–593.
- Terai, C. R., C. S. Bretherton, R. Wood, and G. Painter (2014), Aircraft observations of aerosol, cloud, precipitation, and boundary layer properties in pockets of open cells over the southeast Pacific, *Atmos. Chem. Phys.*, *14*(15), 8071–8088.
- Wang, J., Y. N. Lee, P. H. Daum, J. Jayne, and M. L. Alexander (2008), Effects of aerosol organics on cloud condensation nucleus (CCN) concentration and first indirect aerosol effect, *Atmos. Chem. Phys.*, *8*(21), 6325–6339.
- Wang, Z., A. Sorooshian, G. Prabhakar, M. M. Coggon, and H. H. Jonsson (2014), Impact of emissions from shipping, land, and the ocean on stratocumulus cloud water elemental composition during the 2011 E-PEACE field campaign, *Atmos. Environ.*, *89*, 570–580.
- Warren, S., C. J. Hahn, J. London, R. M. Chervin, and R. L. Jenne (1986), Global distribution of total cloud cover and cloud types over land, NCAR Tech. Note NCAR/TN-273+STR, 29 pp. + 200 maps, Natl. Cent. for Atmos. Res., Boulder, Colo.
- Wood, R. (2012), Stratocumulus Clouds, *Mon. Weather Rev.*, *140*(8), 2373–2423.
- Youn, J. S., E. Crosbie, L. C. Maudlin, Z. Wang, and A. Sorooshian (2015), Dimethylamine as a major alkyl amine species in particles and cloud water: Observations in semi-arid and coastal regions, *Atmos. Environ.*, *122*, 250–258.
- Zhang, J. L., and J. S. Reid (2006), MODIS aerosol product analysis for data assimilation: Assessment of over-ocean level 2 aerosol optical thickness retrievals, *J. Geophys. Res.*, *111*, D22207, doi:10.1029/2005JD006898.